Wall and Roos[17] disagree with ours.) These differences could arise from failures in the basic model assumptions or could represent the effect of neglected distortions produced by the average potential. The validity of our data in the 40-MeV region is supported by the results for the water target but is weakened by the failure of the experiment to differentiate between various secondary charged particles.

This experiment supports the hypothesis that continuum cross sections are predictable by some intranuclear-cascade model down to energies where the proton wavelength $\lambda\!\!\!^{-}$ is about the size of a target nucleon. From limited data, the model seems as applicable to light nuclides as to medium-weight ones. These tentative findings could be illuminated by going to lower energies in both incident and secondary particles, by studying the back angles more carefully, by measuring at enough angles to allow reasonable integrals over solid angle, and by clearly identifying the particle type of all secondaries.

## ACKNOWLEDGMENTS

We are indebted to A. M. Koehler and his crew for helping us utilize the Harvard University Cyclotron, and to the U. S. Office of Naval Research for supporting the costs of our machine use. We thank R. L. Cowperthwaite and P. M. Aebersold for extensive help in analysis and computation, and Hugo Bertini for his many explanations of cascade-plus-evaporation theory and practice. We depended upon Floyd Glass for the design of a stable time-to-amplitude converter, upon Vern McKay and Hugh Brashear for the design of detectors, upon T. Sliski for the mechanical apparatus, and upon support personnel for their careful assistance.

PHYSICAL REVIEW VOLUME 167, NUMBER 4 20 MARCH 1968

# Measurements and Distorted-Wave Born-Approximation Analyses of Some 13.9-MeV Differential Cross Sections for the $N^{14}(He^3,\alpha)N^{13}$ Reactions*

B. T. Lucas,† D. R. Ober, and O. E. Johnson

*Department of Physics, Purdue University, Lafayette, Indiana*

(Received 19 October 1967)

The $(He^3,\alpha)$ differential cross sections leading to the ground and 2.367-, (3.51+3.56)-, 6.38-, and (7.18+7.42)-MeV states of $N^{13}$ have been measured at an incident $He^3$ energy of 13.9 MeV using silicon surface-barrier detectors and a conventional electronic spectrometer system. Energy spectra were accumulated at 2.5° intervals over a laboratory angular range 17.5°–90° and at 5° intervals from 90° to 170°. The experimental differential $(He^3,\alpha)$ cross sections corresponding to states in $N^{13}$ at 0, 2.367, 6.38, and (7.18+7.42) MeV exhibit a pronounced oscillatory structure, suggesting that a direct-reaction mechanism is dominant. The composite cross section corresponding to the transitions leading to the (3.51+3.56)-MeV doublet has a somewhat washed-out structure. All angular distributions display a definite forward-angle peaking, and those leading to the ground and 2.367- and (3.51+3.56)-MeV states of $N^{13}$ show evidence of strong backward-angle peaking. The transitions leading to the odd-parity states in $N^{13}$ appear to be considerably enhanced relative to those leading to the even-parity states. The angular distributions corresponding to the transitions to the ground and 2.367- and 6.38-MeV states have been analyzed within the framework of the zero-range distorted-wave theory using a simple knockout model. The use of cutoff radii equal to or slightly larger than the nuclear radius was necessary in order to obtain reasonably good representations of the experimental data.

## I. INTRODUCTION

In several previous investigations of the $N^{14}(He^3,\alpha)$-$N^{13}$ reactions,[1–3] it was observed that the differential cross section for producing the negative-parity ground state of $N^{13}$ is considerably greater than that for the production of the positive-parity state at 2.367 MeV. Furthermore, in two of these studies,[1,2] it was found that the composite differential cross section corresponding to the unresolved $\alpha$-particle groups associated with the closely spaced (3.51+3.56)-MeV doublet in $N^{13}$ is approximately equal to that for producing the ground state. The results from less complete studies[4,5] at other energies, in which the cross sections were measured at

* Work supported in part by the U. S. Atomic Energy Commission.

† Present address: 1713 Myrtle Avenue, Whiting, Ind.

[1] I. J. Taylor, F. de S. Barros, P. D. Forsyth, A. A. Jaffe, and S. Ramavataram, Proc. Phys. Soc. (London) **A75**, 772 (1960).

[2] K. P. Artemov, V. Z. Goldberg, B. I. Islamov, V. P. Rudakov, and I. N. Serikov, Yadern. Fiz. **1**, 1019 (1965) [English transl.: Soviet J. Nucl. Phys. **1**, 726 (1965)].

[3] A. R. Knudson and F. C. Young, Bull. Am. Phys. Soc. **12**, 502 (1967).

[4] A. Gallmann, D. E. Alburger, D. H. Wilkinson, and F. Hibou, Phys. Rev. **129**, 1765 (1963).

[5] T. E. Young, G. C. Phillips, R. R. Spencer, and D. A. A. S. N. Rao, Phys. Rev. **116**, 962 (1959).

only a few isolated angles, are in substantial agreement with these findings. The parities of the 3.51- and 3.56-MeV states are now known to be negative and positive, respectively.[6] In the light of recent experimental results,[7–9] the state in $N^{13}$ at 7.42 MeV, which had been previously assigned a spin and parity of $\frac{5}{2}^+$, has now been assigned a negative parity. It has been suggested[10] that this might be the missing $\frac{5}{2}^-$ level predicted from intermediate-coupling shell-model calculations.[11,12] If a correlation exists between the relative magnitudes of the differential cross sections for the $N^{14}(He^3,\alpha)N^{13}$ reactions and the parity of the final state, then one might expect to observe a relatively intense $\alpha$-particle group associated with the 7.4-MeV state. Although an earlier investigation[2] revealed a strong $\alpha$-particle group corresponding to a state near 7 MeV, it was tentatively identified as a composite group associated with the 6.91- and 7.18-MeV states. Since experimental evidence indicates that both of these states are of positive parity,[8] it is interesting to speculate as to whether this group might have been actually associated with the 7.4-MeV state of $N^{13}$. An energy-level diagram for the states in $N^{13}$ below 8 MeV is given in Fig. 1.

The studies of the $N^{14}(He^3,\alpha)N^{13}$ reactions at 5.2 MeV[1] and at 17.4, 25.4, and 36.6 MeV[2] yielded angular distributions that are strongly peaked in the forward direction, suggesting that a direct-reaction mechanism is dominant. To date no distorted-wave analyses of these of these data have been reported; however, the 5.2-MeV angular distributions of Taylor *et al.*[1] corresponding to the production of the ground and (3.51+3.56)-MeV states have been analyzed in terms of the plane-wave Butler theory.[13] Moderately good fits to the data were obtained. It is interesting to note that of the alternative reaction mechanisms, pickup and knockout, the former is generally believed to be dominant. It has been pointed out, however, that on the basis of shell-model descriptions, the positive-parity states in $N^{13}$ cannot be produced by the simple pickup of a single nucleon.[14] On the other hand, the knockout model, assuming simple cluster-model representations for the initial and final nuclei, does not explicitly exclude these transitions. Analyses in terms of this model have not been previously reported.

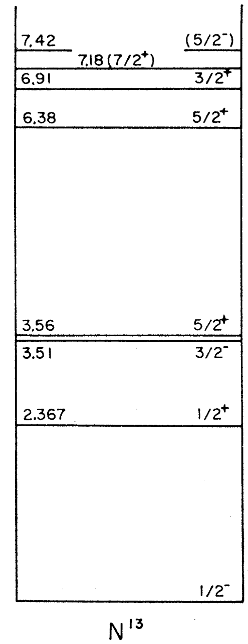


FIG. 1. The energy levels of $N^{13}$ below 8 MeV. Information pertaining to levels below 7-MeV excitation are taken from Ref. 6. Spin and parity assignments for the other levels shown are taken from Refs. 8 and 12.

The present investigation was undertaken to (a) study the suggested systematic enhancement of the cross sections for the production of the negative-parity states in $N^{13}$, (b) measure the 13.9-MeV $(He^3,\alpha)$ angular distributions corresponding to several of the low-lying states in $N^{13}$, and (c) analyze the experimental angular distributions in terms of a simple distorted-wave Born-approximation (DWBA) knockout model.

## II. EXPERIMENTAL PROCEDURE

A description of the Purdue University cyclotron facility may be found in an earlier paper.[15] The energy of the $He^3$ beam at the target was 13.95 MeV, with an estimated rms spread of 40 keV.

The single target used in this experiment was prepared by the vacuum evaporation of Melamine ($N_6C_3H_6$) onto a thin (15 $\mu$g/cm$^2$) Formvar film. The total measured target thickness was $546\pm20$ $\mu$g/cm$^2$, of which $346\pm13$ $\mu$g/cm$^2$ was nitrogen.

Four charged-particle spectra were accumulated simultaneously, using four silicon surface-barrier counters[16] rigidly mounted in a multidetector assembly with defining apertures spaced 10° apart, an electronic gating and routing system, and a two-dimensional pulse-height analyzer. The defining apertures in the detector assembly were $\frac{5}{32}$ in. diameter. For each detector, the solid angle with respect to the target was $0.664\times10^{-3}$ sr and the azimuthal acceptance angle was 1.7°. The over-all

[6] Unless otherwise specified, the level structure and individual level properties for $N^{13}$ in the following compilation will be assumed; see T. Lauritsen and F. Ajzenberg-Selove, *Energy Levels of Light Nuclei-May 1962* (National Academy of Sciences–National Research Council, Washington, D. C.). In those instances where revised and/or more detailed information is relevant, appropriate references will be made.

[7] N. Nikolic, L. J. Lidofsky, and T. H. Kruse, Phys. Rev. **132**, 2212 (1963).

[8] F. C. Barker, G. D. Symons, N. W. Tanner, and P. B. Treacy, Nucl. Phys. **45**, 449 (1963).

[9] G. G. Shute and A. M. Baxter, Nucl. Phys. **83**, 460 (1966).

[10] F. C. Barker, Nucl. Phys. **28**, 96 (1961).

[11] D. Kurath, Phys. Rev. **101**, 216 (1956).

[12] F. C. Barker, Nucl. Phys. **45**, 467 (1963).

[13] S. T. Butler, Phys. Rev. **106**, 272 (1957).

[14] E. K. Warburton and J. N. McGruer, Phys. Rev. **105**, 639 (1957).

[15] B. T. Lucas, S. W. Cosper, and O. E. Johnson, Phys. Rev. **133**, B963 (1964).

[16] The detector biases were adjusted so as to effectively discriminate against the deuterons produced in the $N^{14}(He^3,d)O^{15}$ reactions.

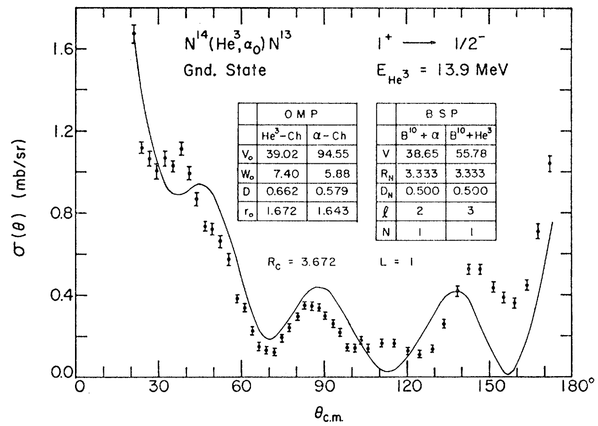


FIG. 2. A comparison of the experimental differential cross sections (solid circles) with the best-fitting DWBA knockout angular distribution (solid curve) for the $N^{14}(He^3,\alpha_0)N^{13}$ reaction. The theoretical curve is normalized to the experimental data so as to achieve a subjective, best over-all fit. Other information in the figure includes the spin and parity of the initial and final nuclei, the bound-state parameters (BSP), the entrance- and exit-channel optical-model parameters (OMP), the cutoff radius ($R_C$), and the value of the angular momentum transfer ($L$). The bars on the experimental points represent the probable errors arising from counting statistics only.

energy resolution of the system was 180–200 keV for the $\alpha$-particle groups of interest.

Energy spectra were accumulated at 2.5° intervals over a laboratory angular range 17.5°–90° and at 5° intervals from 90° to 170°. The ranges of the probable errors in the differential cross sections arising from counting statistics and background subtraction are 3–5% for the ground-state group, 10–20% for the 2.367-MeV group, 4–6% for the (3.51+3.56)-MeV doublet, 10–15% for the 6.38-MeV group, and 2–5% for the (7.18+7.42)-MeV doublet. The estimated probable systematic error in the absolute cross section arising from uncertainties in target thickness, beam integration, and experimental geometry is ±15%.

TABLE I. The integrated 13.9-MeV cross sections for the $N^{14}(He^3,\alpha_n)N^{13}$ reactions leading to the various final states in $N^{13}$.

| Final State No. | $J_F{}^{\pi}$ [a] | $E_x$ (MeV) | Angular range[b] (deg) | $\sigma$ (mb) |
|---|---|---|---|---|
| 0 | $\frac{1}{2}^-$ | 0 | 20.7–105.8 | 3.442 |
| | | | 20.7–171.9 | 4.696 |
| 1 | $\frac{1}{2}^+$ | 2.367 | 23.9–106.4 | 0.456 |
| | | | 23.9–174.0 | 0.695 |
| 2+3 | $\frac{3}{2}^-,\frac{5}{2}^+$ | 3.51,3.56 | 24.0–106.8 | 4.262 |
| | | | 24.0–172.0 | 6.552 |
| 4 | $\frac{5}{2}^+$ | 6.38 | 21.4–107.9 | 1.367 |
| 6+7 | $\frac{7}{2}^+,\frac{5}{2}^-$ [c] | 7.18,7.42 | 21.5–108.4 | 11.858 |
| | | | 21.5–164.5 | 18.336 |

[a] The spin and parity assignments, and the excitation energies of the states in $N^{13}$, have been taken from Ref. 6 except where specifically noted otherwise.
[b] Those integrated cross sections corresponding to a smaller angular range than that covered by the experimental data were included to facilitate comparisons of relative intensities.
[c] The results of more recent investigations favor these assignments (see Refs. 7–9, and 12).

## III. EXPERIMENTAL RESULTS

The experimental values of the differential cross sections for the $N^{14}(He^3,\alpha_n)N^{13}$ reactions which leave $N^{13}$ in its ground state ($n=0$), 2.367-MeV state ($n=1$), and 6.38-MeV state ($n=4$) are shown in Figs. 2, 3, and 4, respectively. The 6.38-MeV state was too weakly excited for angles larger than about 95° to permit the extraction of a reliable cross section. The experimental resolution of the spectrometer system was not sufficient to resolve the (3.51+3.56)- and (7.18+7.42)-MeV doublets; therefore separate angular distributions could not be determined. The composite angular distributions for the $\alpha_{2+3}$ and $\alpha_{6+7}$ doublets are shown in Fig. 5.

The integrated cross sections for the various angular distributions and the angular ranges over which the integrations were performed are shown in Table I.

## IV. ANALYSIS

### A. General

In the distorted-wave formalism, the transition amplitude for the ($He^3$,$\alpha$) reaction may be written

$$A_{He^3,\alpha}(\mathbf{K}_I,\mathbf{K}_F)=\langle\Phi_F{}^{(-)}(\mathbf{K}_F)\varphi_\alpha\varphi_F|\,V_{\alpha,F}-\bar{V}_{\alpha,F}\times|\,\Phi_I{}^{(+)}(\mathbf{K}_I)\varphi_{He^3}\varphi_I\rangle, \quad (1)$$

where $\Phi_I{}^{(+)}$ and $\Phi_F{}^{(-)}$ are the optical-model (OM) wave functions describing the relative motion of the particles in the entrance and exit channels, respectively. The wave functions $\varphi_{He^3}$ and $\varphi_\alpha$ describe the internal structure of the $He^3$ and $\alpha$ particles, while $\varphi_I$ and $\varphi_F$ are the wave functions for the target and residual nuclei, respectively. $V_{\alpha F}$ represents the total interaction between the $\alpha$ particle and the residual nucleus. $\bar{V}_{\alpha F}$ is that part of the total interaction assumed to adequately describe the elastic scattering, and is generally taken to be the OM potential.

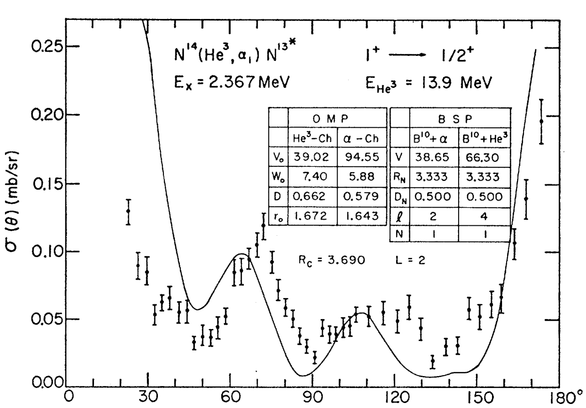


FIG. 3. A comparison of the experimental differential cross sections (solid circles) with the best-fitting DWBA knockout angular distribution (solid curve) for the $N^{14}(He^3,\alpha_1)N^{13}$ reaction. The general format for this figure is the same as that of Fig. 2. $E_x$ is the excitation energy of the final state.

In the present analyses, a knockout model as formulated by Tobocman[17] was used, and numerical calculations were performed using the direct-reaction code developed by Gibbs *et al.*[18] In this model the interaction is simplified by assuming that

$$V_{\alpha,F}-\bar{V}_{\alpha,F}=V_{\alpha,\mathrm{He}^3}=v_0\delta(\mathbf{r}_{\mathrm{He}^3}-\mathbf{r}_\alpha). \qquad (2)$$

The target (residual) nucleus was assumed to consist of an $\alpha$ particle ($He^3$ particle) bound to a $B^{10}$ core. The quantum state of the relative motion of the initial (final) two-body bound system is characterized by the relative orbital angular momentum and radial quantum numbers $l$ ($l'$) and $N$ ($N'$), respectively. The selection rules for the allowed values of $l$, $l'$ and the angular momentum transfer $L$ may be found elsewhere.[19] The allowed values of these quantum numbers for the various states of interest in $N^{13}$ are given in Table II. The value of $N$, the radial quantum number of the initial state, was chosen to be unity since this corresponds to the lowest bound state for a given $l$. The radial quantum numbers associated with the states in the residual nucleus were chosen so as to produce similar bound-state potential-well depths for all final states of interest. It should be pointed out that the expression for the differential cross section involves an incoherent sum over all the allowed $L$ values, and each term corresponding to a particular $L$ value consists of a coherent sum over those values of $l$ and $l'$ consistent with the selection rules for that particular $L$. On physical grounds, however, it can be argued that only single values of $l$ and $l'$ need be considered.[19]

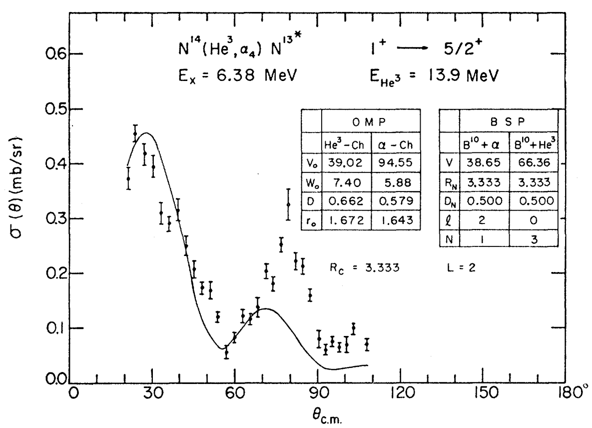


FIG. 4. A comparison of the experimental differential cross sections (solid circles) with the best-fitting DWBA knockout angular distribution (solid curve) for the $N^{14}(He^3,\alpha_4)N^{13}$ reaction. The format for this figure is the same as that for Fig. 3.

[17] W. Tobocman, *Theory of Direct Nuclear Reactions* (Oxford University Press, London, 1961).

[18] W. R. Gibbs, V. A. Madsen, J. A. Miller, W. Tobocman, E. C. Cox, and L. Mowry, *Direct Reaction Calculation, NASA TN D-2170* (National Aeronautics and Space Administration, Washington, D. C., 1964).

[19] B. B. Srivastava, S. W. Cosper, and O. E. Johnson, Phys. Rev. **153**, 1221 (1967).

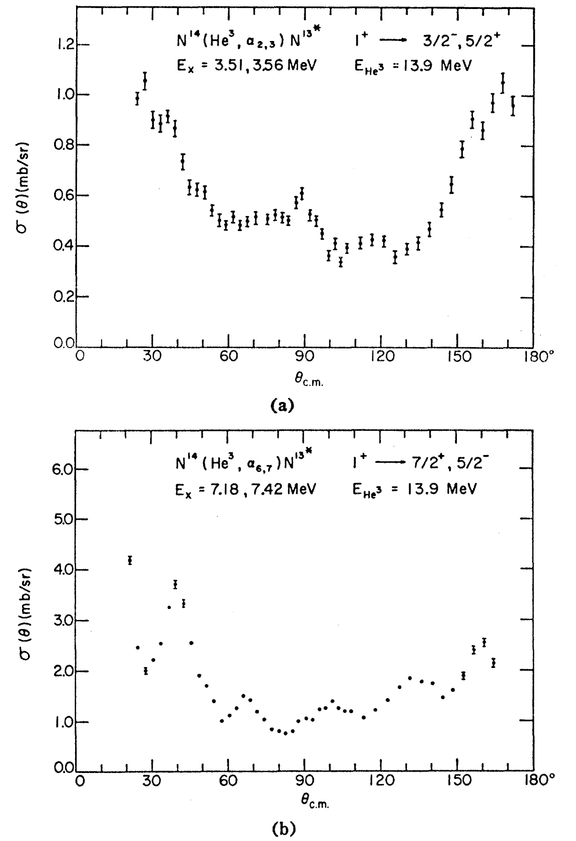


FIG. 5. The composite differential cross sections for (a) the $N^{14}(He^3,\alpha_{2,3})N^{13}$ reactions and (b) $N^{14}(He^3,\alpha_{6,7})N^{13}$ reactions. The bars on the experimental points indicate the probable errors arising from counting statistics only.

The OM parameters used to describe the relative motion in the entrance channel were derived from analyses of the data for 13.9-MeV $He^3$ particles elastically scat-

TABLE II. The allowed values of the bound-state quantum numbers and the corresponding potential-well depths for the two-body systems representing the initial ($B^{10}+\alpha$) and final ($B^{10}+He^3$) nuclear states in the knockout-model description of the $N^{14}(He^3,\alpha_n)N^{13}$ reactions ($n=0$, 1, and 4).

| State | $J_I^\pi$ | $J_F^\pi$ | $l$ | $l'$ | $L$ | $N$ | $N'$ | $V$ (MeV) | $V'$ (MeV) |
|---|---|---|---|---|---|---|---|---|---|
| 0 | $1^+$ | $\frac{1}{2}^-$ | 2 | 3 | 1 | 1 | 1 | 38.65 | 55.78 |
| | | | 4 | 3 | 1 | 1 | 1 | 62.10 | 55.78 |
| 1 | $1^+$ | $\frac{1}{2}^+$ | 2 | 2 | 0,2 | 1 | 2 | 38.65 | 69.87 |
| | | | 2 | 4 | 2 | 1 | 1 | 38.65 | 66.30 |
| | | | 4 | 2 | 2 | a | | | |
| | | | 4 | 4 | 0,2 | a | | | |
| 4 | $1^+$ | $\frac{5}{2}^+$ | 2 | 0 | 2 | 1 | 3 | 38.65 | 66.36 |
| | | | 2 | 2 | 0,2,4 | 1 | 2 | 38.65 | 65.16 |
| | | | 2 | 4 | 2,4 | 1 | 1 | 38.65 | 61.84 |
| | | | 2 | 6 | 4 | a | | | |
| | | | 4 | 0 | 4 | a | | | |
| | | | 4 | 2 | 2,4 | a | | | |
| | | | 4 | 4 | 0,2,4 | a | | | |
| | | | 4 | 6 | 2,4 | a | | | |

[a] Although these combinations of quantum numbers were not specifically investigated, arguments are presented in the text to rule them out as possible assignments.

TABLE III. The sets of OM parameters investigated in the analysis of the $N^{14}(He^3,\alpha_0)N^{13}$ reaction.[a]

| Reaction energy | Set No. | $V_0$ (MeV) | $W_0$ (MeV) | $D$ (F) | $r_0$ (F) |
|---|---|---|---|---|---|
| $N^{14}(He^3,He^3)N^{14}$ | 1 | 39.02 | 7.40 | 0.662 | 1.672 |
| 13.9 MeV | 2 | 74.09 | 16.05 | 0.538 | 1.726 |
| | 3 | 126.94 | 22.14 | 0.527 | 1.616 |
| $N^{14}(\alpha,\alpha)N^{14}$ | 4 | 24.87 | 4.22 | 0.594 | 1.864 |
| 19.2 MeV | 5 | 54.87 | 5.17 | 0.569 | 1.748 |
| | 6 | 94.55 | 5.88 | 0.579 | 1.643 |
| | 7 | 149.79 | 7.03 | 0.572 | 1.537 |

[a] Although all of these sets of OM parameters resulted from analyses in the present investigation, the elastic $\alpha$-particle scattering cross sections used are those of Ref. 21.

tered from $N^{14}$.[20] Correct descriptions of the relative motion in the exit channels would require OM parameters corresponding to $\alpha$-particle scattering from $N^{13}$ at various energies from 20 to 28 MeV. Since these were not available, the parameters used to describe the exit channel were derived from an analysis of the data for 19.2-MeV $\alpha$ particles elastically scattered from $N^{14}$.[21] The sets of OM parameters used in these analyses are listed in Table III. They correspond to a four-parameter Saxon-Woods potential of the form

$$U(r)=-(V_0+iW_0)/(e^x+1)\,, \quad (3)$$

where

$$x=(r-r_0A^{1/3})/D. \quad (4)$$

A Coulomb potential corresponding to a uniformly charged sphere of radius $1.2A^{1/3}$ F was also assumed.

The bound-state wave functions $\varphi_I$ and $\varphi_F$ for the representative two-body systems were calculated assuming a two-body potential consisting of a real, attractive potential of a Saxon-Woods shape and a repulsive Coulomb potential corresponding to a uniformly charged sphere. The shape parameters for the Saxon-Woods potential, $R_N$ and $D_N$, were assigned fixed values of 3.333 and 0.500 F, respectively. The radius of the Coulomb potential was also assigned a fixed value of 3.333 F. The depth of the Saxon-Woods potential, $V$, is uniquely determined once the radial and orbital angular momentum quantum numbers, and the binding energy, are specified. Agreement between the experimental and theoretical cross sections could not be obtained without the use of a cutoff radius and the introduction of an adjustable normalization constant. Fits were obtained using cutoff radii larger than or equal to the nuclear radius; values of $R_C<R_N$ were not extensively investigated.

The "best" set of parameter values was taken to be that set which yielded the best subjective fit over the entire angular range covered by the experimental data.

[20] The data upon which the optical-model analyses were performed were recently measured at this laboratory.

[21] For a description of the measurements and the experimental results, see W. D. Ploughe, Phys. Rev. 122, 1232 (1961).

### B. Procedures

The $(He^3,\alpha_0)$ angular distribution was chosen for the initial fitting attempts principally because of the relatively small number of combinations of allowed $(l,l',L)$ values associated with it (see Table II). The initial-state relative orbital angular momentum quantum number was chosen to be $l=2$, since it corresponds to the lowest allowed bound state for a given $N$. Previous and present experience with this model has shown that the shape of the theoretical cross section is not very sensitive to the values of $N$ and $N'$ when $R_C\geqslant R_N$. Consequently, although all 12 possible combinations of the entrance- and exit-channel OM parameters listed in Table III were investigated for values of $R_C$ in the range from $R_N$ to $R_N+1$ F, it was not necessary to consider all possible $(N,N')$ combinations in each case. For the ranges and combinations of parameters investigated, the best fit results from using OM parameter set Nos. 1 and 6 of Table III with $R_C=3.672$ F. A comparison of the resulting theoretical curve and the experimental data is shown in Fig. 2.

Since the relative quality of the fits provided no basis for the selection of the values of $N$ and $N'$, the assignments $N=N'=1$, which correspond to the lowest energy bound states for a given $l$ value, were made. Calculations taking $l=4$ indicated that the shapes of the calculated angular distributions for $l=2$ and 4 were identical. Since this $l$ ambiguity could not be resolved on the basis of the relative quality of the fits achieved, the assignment of $l=2$, which corresponds to the lower energy bound state in the $B^{10}+\alpha$ system, was made.

In the case of the $(He^3,\alpha_1)$ reaction, this model allows two values for both $l$ and $l'$; however, the assignment of $l=2$, as described in the analysis of the $(He^3,\alpha_0)$ data, reduces the number of possibilities. The first series of calculations was performed with $l'=2$; $L=0$, 2; $N=1$; $N'=2$; and cutoff radii values from 3.333 to 4.047 F. Although the $L=2$ component of the calculated cross section had the same general shape as the experimental angular distribution, the dominant $L=0$ component had a distinctly different shape. The calculations performed using $l'=4$, $L=2$, and $N'=1$ yielded cross sections which were very similar to the $L=2$ component of the cross section for $l'=2$. The best fit was achieved for $R_C=3.690$ F and is shown in Fig. 3.

The analysis of the $(He^3,\alpha_4)$ angular distribution is complicated by the four allowed values of $l'$. A series of calculations was performed with $l=2$; $l'=0$, 2, 4; and all the allowed values of $L$. For each of the various combinations of quantum numbers, the cutoff radius was varied from 3.333 to 3.710 F. In those cases for which multiple values of the angular momentum transfer are allowed, individually, the $L=0$ and $L=4$ contributions bear little resemblance to the experimental data; however, the $L=2$ cross section reproduces the experimental cross section fairly well. The shape of the component of the angular distribution for a given $L$ value was found to be insensitive to the value of $l'$; consequently, the combination involving $l=2$ and $l'=6$ could be eliminated without further calculation. The angular distribution corresponding to $l'=0$, $L=2$, and $R_C=R_N=3.333$ F best reproduces this experimental cross section (see Fig. 4).

## V. DISCUSSION

In the present investigation, it was found that the enhancement of the cross section for the production of the negative-parity $N^{13}$ ground state relative to that for the production of the positive-parity 2.367-MeV state, which had been previously reported for incident energies of 5.2 MeV,[1] 16–17 MeV,[2] and 4.5–7 MeV,[3] persists at 13.9 MeV. In addition, the present measurements show that the production cross section for the 6.38-MeV state of $N^{13}$ is relatively small and suggest that the major component of the composite cross section for the production of the 7.18- and 7.4-MeV states of $N^{13}$ corresponds to the transition to the higher-energy final state. These observations lend further credence to the suspected correlation between the transition strength and the final-state parity. Of course, such a correlation might be expected if the simple shell-model representation is assumed for the states in question, since then, as indicated previously, a simple pickup reaction will not lead to positive-parity final states and a somewhat more complicated reaction mechanism, presumably knockout, will be responsible for their production.

It should also be noted that the angular distributions corresponding to closely neighboring states of different parities have minima and maxima of opposite phase (compare the angular distribution $\alpha_0$ with $\alpha_1$ and $\alpha_4$ with $\alpha_{6+7}$).

The features of the composite $\alpha_{2+3}$ angular distribution may be readily interpreted on the basis of the two preceding observations concerning the correlation of relative intensities and phases of the extrema in the angular distributions with the parity of the final state. The strong peaking at forward and backward angles and the maximum at 90° may be associated with the cross section for the production of the $\frac{3}{2}^-$ state at 3.51 MeV, which is presumably the dominant contribution, while the rather washed-out structure around 70° and 115° results from the superposition of the relatively weaker maxima in the angular distribution associated with the $\frac{5}{2}^+$ state at 3.56 MeV. It should also be noted that, in contrast to the present result, the $\alpha_{2+3}$ angular distributions measured at various energies in the range from 4.5–7 MeV have been reported[3] to be approximately isotropic.

The calculated curves reproduce all the general features of the $\alpha_0$ and $\alpha_1$ angular distributions, but in the case of the $\alpha_4$ angular distribution the correspondence is not quite as good. However, in attempting to associate either a pickup or a knockout mechanism with the production of the various final states, caution must be exercised. Our experience in analyses using the simple knockout and pickup models of Tobocman[17] supports the conclusion that the shapes of the calculated angular distributions are insensitive to the bound-state quantum numbers when the cutoff radius is equal to or larger than the nuclear radius, provided that the allowed angular momentum transfer values are the same. This observation is in accord with Austern's assertion that, for strongly absorbed particles, the shapes of the angular distributions predicted by zero-range distorted-wave theory are determined primarily by the OM wave functions.[22] It follows that the $\alpha_0$ angular distribution could be well reproduced by the simple pickup model. Although these analyses certainly do not provide a definitive basis for the identification of the mechanism responsible for the production of the various final states, a consistent interpretation would be to associate the production of the positive- and negative-parity final states with the knockout and the pickup mechanisms, respectively. On the other hand, the success of these models in reproducing the features of the angular distributions does suggest that the direct-reaction mechanism is dominant in these reactions at 13.9 MeV.

## ACKNOWLEDGMENTS

The authors are especially grateful to Dr. B. B. Srivastava for many useful discussions concerning the analysis of the experimental data. Special thanks are also due to Dr. D. J. Tendam for his assistance in producing the $He^3$ beam. The efforts of K. R. Runck and F. G. Hobaugh in the operation and assistance in the maintenance of the cyclotron throughout the course of these measurements are greatly appreciated.

[22] N. Austern, in *Selected Topics in Nuclear Theory* (International Atomic Energy Agency, Vienna, 1963), p. 30.